# Planar biaxial tensile testing of weft-knitted textiles with varying knit architectures

Christidi, Nikoletta; Louter, Christian; Popescu, Mariana

**DOI**
10.1016/j.conbuildmat.2025.144482

**Publication date**
2025

**Document Version**
Final published version

**Published in**
Construction and Building Materials

**Citation (APA)**
Christidi, N., Louter, C., & Popescu, M. (2025). Planar biaxial tensile testing of weft-knitted textiles with varying knit architectures. *Construction and Building Materials*, *504*, Article 144482. https://doi.org/10.1016/j.conbuildmat.2025.144482

Construction and Building Materials 504 (2025) 144482

Contents lists available at ScienceDirect

Construction and Building Materials

journal homepage: www.elsevier.com/locate/conbuildmat

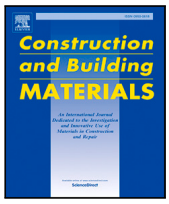

# Planar biaxial tensile testing of weft-knitted textiles with varying knit architectures

Nikoletta Christidi [a,*], Christian Louter [a], Mariana Popescu [a,b]

[a] Faculty of Civil Engineering and Geosciences, Delft University of Technology, Stevinweg 1, Delft, 2628 CN, The Netherlands
[b] Massachusetts Institute of Technology, 77 Massachusetts Ave, Cambridge, MA 02139, USA

ARTICLE INFO

*Keywords:*
Tensile structures
Knitted textiles
Knit architecture
Biaxial tensile testing
Material characterization
Elastic properties

ABSTRACT

Textiles are widely used in tensile structures due to their low weight, flexibility, and ability to span large areas efficiently through membrane action. Weft-knitted textiles, in particular, offer customization at a unit level, enabling the creation of locally programmable, 3D-shaped, continuous membranes. However, their mechanical characterization remains challenging, despite its importance for structural applications such as flexible formwork. This study examines the biaxial elastic properties of CNC weft-knitted textiles, focusing on the influence of knit architecture on their mechanical response. A custom biaxial tensile testing setup was developed to test three knitting patterns – interlock, tuck, and hexagonal – under three strain ratios (1:2, 1:1, and 2:1). Results show that stiffness varies significantly with knitting pattern and direction, reflecting asymmetries in textile microstructure. Strain distribution was also found to be non-uniform, with lower strains at the core than on the edges, highlighting the role of boundary conditions. Beyond providing insights into weft-knitted textile behaviour, this study contributes to an experimental framework for biaxial stiffness evaluation. The methodology serves as a proof-of-concept framework for the biaxial testing, test preparation, and result interpretation for knitted textiles, as well as for developing low-cost biaxial testing setups. These findings are particularly relevant for architectural and construction applications, where understanding the mechanical behaviour of knitted textiles is essential for structural integrity and design optimization.

## 1. Introduction

Textiles are lightweight, flexible, and they can efficiently cover large spans acting in pure tension [1], which is why they are widely used in tensile structures. While woven textiles (Fig. 1a) are the most common, due to their stable configuration [2] and relatively predictable behaviour, weft-knitted textiles (Fig. 1b) have also been gaining attention from researchers in the past two decades. This is because they can be specified at a unit (stitch) level, making it possible to create heterogeneous, 3D-shaped, continuous membranes with programmable local features and properties [3,4]. Using specialized computer numerical control (CNC) knitting machines enables the efficient production of such textiles suitable for large-scale applications, thereby broadening the scope of knitted textiles in contemporary architectural design and construction [5].

While precise textile specification is achievable through CNC knitting, designing tailored knitted textiles for structural applications remains a complex task. This complexity is attributed to the interplay of factors such as material properties of the yarns used, knitting machine settings, and knit architecture, which refers to the matrix of local stitch types and knitting operations used during fabrication. The knit architecture of a textile significantly influences its initial geometry, size, and elasticity, even when made from the same yarn material. These factors affect the ability of the textile to stretch to a target geometry. They also influence its mechanical behaviour under various loading conditions once the target geometry is achieved, ultimately shaping its engineering potential [6].

This fact is particularly relevant in flexible formwork applications, where textiles deform under the load of concrete or other building materials. Their local deformation is governed not only by prestress and yarn material but also by the local knit architecture, which dictates force distribution and determines how the textile adapts to external loads (Fig. 2). Therefore, understanding the effect of knit architecture on the mechanical properties of textiles is essential for predicting and analysing their structural behaviour in building applications [7].

The mechanical properties of a textile can be obtained through physical testing. More specifically, for tensile and elastic properties, uniaxial and biaxial tensile testing can be conducted. Since loads are carried by textiles through in-plane membrane action, usually in the

* Corresponding author.
*E-mail address:* N.Christidi@tudelft.nl (N. Christidi).

https://doi.org/10.1016/j.conbuildmat.2025.144482
Received 16 April 2025; Received in revised form 4 September 2025; Accepted 8 November 2025
Available online 27 November 2025

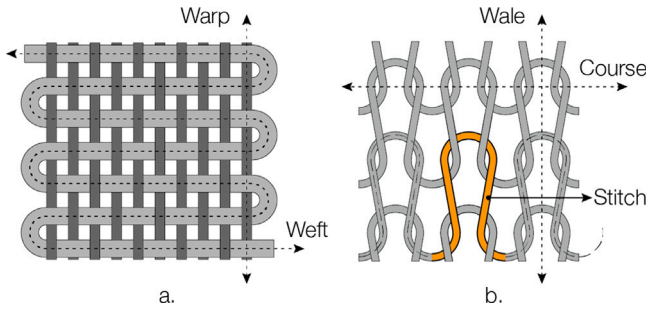


**Fig. 1.** Textile types: (a) Woven textile; (b) Weft-knitted textile.

form of biaxial stress states [9], design and analysis of tensile structures requires knowledge of biaxial stiffness parameters, rendering biaxial testing necessary in this context.

Planar biaxial tensile testing involves simultaneously pulling a specimen in two perpendicular to each other directions by controlling the force, strain or displacement applied at its boundaries. This type of testing, introduced in the 1950s, allows for the introduction of in-plane external forces independently in two directions, a process which closely resembles the real in-situ conditions [10]. Therefore, it is considered to be the most reliable testing method for the characterization of structural membranes, such as coated and uncoated fabrics.

While European and international test standards exist for determining the biaxial tensile properties of woven textiles [11–14], no equivalent standards are currently available for knitted textiles [15,16]. A key difference between the two lies in the specimen preparation process. Unlike woven textiles, where specimens can be cut to the required size from a larger textile piece, knitted textiles cannot be cut without risking unravelling the entire piece [16]. Securing the edges with additional seams, such as overlock stitching [17], is not desirable, as it would significantly alter boundary stiffness. As a result, specimens must be knitted directly into the desired dimensions, requiring a different approach to specimen preparation, testing methodology, and standardization.

In regards to woven textiles, the effect of the weave architecture on their mechanical properties has been investigated by many researchers, as presented in a 2022 review by Begum and Milašius [6]. Similar attempts have been made for knitted textiles. Studies by Choi and Ashdown [18] and Brad and Dinu [19] showed that tensile properties generally improve with knit density caused by variations in the knit architecture. Semnani [20] also revealed that the rib structure enhances tensile strength. Other researchers [21–24] compared the tensile properties of textiles with different knitting patterns (as uniform knit architectures are commonly referred to), but with a focus on the effect of the yarn material.

Comprehensive studies on the influence of knit architecture on the mechanical properties of textiles in the context of tensile structures remain scarce. Research in this field has primarily focused on knitwear applications, where materials such as cotton and nylon are commonly studied, rather than high-strength materials more suitable for structural applications, such as polyester. Notable exceptions include the works of Tamke et al. [16,17] and Monticelli et al. [15], who not only highlighted the need for design-driven testing approaches tailored to knitted textiles, but also conducted experimental tensile testing to assess their mechanical behaviour for architectural use. Nevertheless, a systematic understanding of the elastic and tensile properties of CNC weft-knitted textiles, as influenced by yarn material and knit architecture, is still lacking. No comprehensive database or predictive models currently exist to establish relationships between these parameters and mechanical performance. Additionally, there are no official standards for the preparation, execution, or interpretation of biaxial tensile testing on weft-knitted textiles. Therefore, the research presented in this paper lays the groundwork for an experimental testing method to characterize the biaxial elastic properties of CNC weft-knitted textiles made from recycled PET, considering variations in knit architecture.

## 2. Methodology

To investigate the influence of knit architecture on the elastic properties of CNC weft-knitted fabrics, biaxial tensile tests were carried out. The process was structured into four phases (Fig. 3):

- **Phase 1:** The design and construction of the biaxial tensile testing setup (Section 2.1).
- **Phase 2:** Specimen preparation, which involved pattern selection, calibration, fabrication, preparation for Digital Image Correlation (DIC), and clamping (Section 2.2).
- **Phase 3:** Execution of the main experimental procedure (Section 2.3).
- **Phase 4:** Data processing and analysis (Section 2.4).

The first phase was completed before the start of the main experimental campaign, which comprised phases 2, 3 and 4. All campaign phases were repeated for each specimen. In total, 27 tests were carried out: 3 strain ratios, 3 knitting patterns, and 3 specimens per strain ratio/knitting pattern combination.

### 2.1. Biaxial tensile testing setup

A custom mechanical biaxial tensile testing setup (Figs. 4, 5) was designed and built to determine the biaxial elastic properties of weft-knitted textiles with varying knit architectures. The setup operated under displacement control, applying tension to the textile specimens in two orthogonal directions, with a maximum force capacity of approximately 150 N. The displacement was induced using four linear actuators mounted on an aluminium frame. Force data was recorded through four load cells (two per axis), while displacement data was captured using four rotary encoders (two per axis) and DIC. The DIC measurements were obtained by analysing photographs taken at each displacement step with a digital camera.

#### 2.1.1. Displacement control

The biaxial testing setup was displacement-controlled, meaning that the displacement of the axes tensioning the specimens could be regulated according to user input in an open loop. Forces were not actively controlled, but measured in real time. This open-loop displacement protocol was deemed more straightforward, compared to a force/tension driven closed-loop protocol [25], and it allowed for control over strain ratios during tensioning. Displacement was applied in discrete steps, each followed by a 3-second pause, resulting in approximately 20 displacement steps per minute. This displacement rate was chosen to maintain a quasi-static loading regime and allow sufficient time for image capturing between steps.

The biaxial stiffness of textiles, including weft-knitted ones, depends on the ratio of applied strain or stress in the two principal directions [9]. In this study, displacement in the Y axis, or, in knitting terminology, wale direction (Fig. 1b), was carried out in predefined steps of 2 mm. Displacement in the X axis, or course direction, varied depending on the tested strain ratio. Overall, three strain ratios were tested: 1:1 (wale step: 2 mm, course step: 2 mm), 1:2 (wale step: 2 mm, course step: 4 mm), and 2:1 (wale step: 2 mm, course step: 1 mm).

Axial displacement of the moving components was achieved using four lead screw-driven linear actuators arranged symmetrically around the centre of the test area. In these actuators, a NEMA23 stepper motor (Fig. 6a) rotated a threaded metal rod, resulting in the outward linear displacement of a metal platform along the X or Y axis, which facilitated the tensioning of the textile. The clamps holding the textile were mounted on these moving platforms. The rotation of the stepper motors


**Fig. 2.** Knitted textiles with distinct knit architectures deforming differently under the same concrete load: (a) Cross miss pattern; (b) Single cross tuck pattern; (c) Double half cardigan pattern. Project and photos by Lucy Flieger [8].

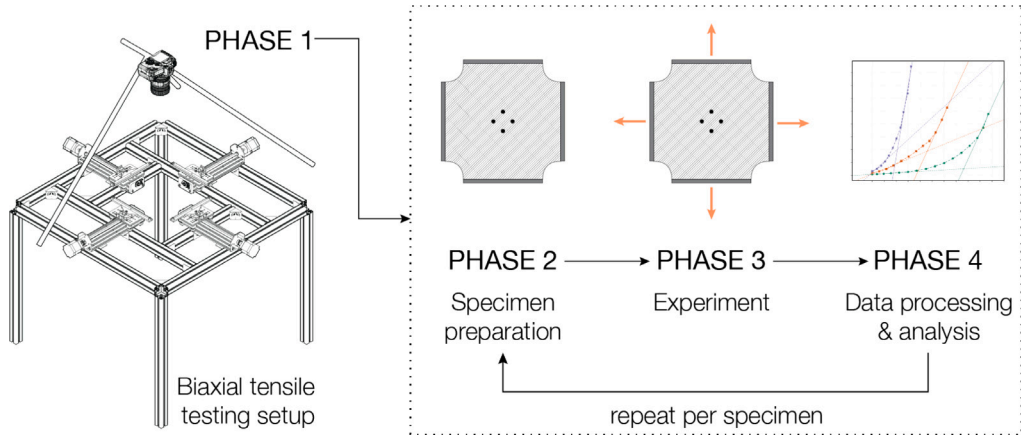


**Fig. 3.** Methodology flow chart: design and construction of biaxial tensile testing setup, specimen preparation, experimental procedure, data processing and analysis.

was controlled via a Teensy microcontroller connected to a laptop. An Arduino programme, loaded onto the microcontroller, provided multiple displacement and data recording options, which were accessed and executed with the help of a Python script.

### 2.1.2. Displacement measurement

The intended displacement, determined by a predefined motor rotation, sometimes does not align with the actual displacement achieved by the setup. This discrepancy can occur, for example, when the movement of the platforms is obstructed, causing the motor to continue spinning without effectively translating the motion. To address this issue, the recorded displacement of the clamps was not based on the rotation of the motor. Instead, it relied on measurements from rotary encoders (Fig. 6b) mounted on the lead screws of the linear actuators. These AMT102-V encoders monitored the rotation of the threaded rods with a specified resolution, determined by the encoders' configuration. The encoder output signal was subsequently converted into a displacement value using the following formula:

$$\text{Displacement} = \frac{\text{Encoder Reading} \times \text{Lead Screw Pitch}}{\text{Pulses per Revolution}}$$

where:

- **Encoder Reading:** The total number of pulses recorded by the encoder,
- **Pulses per Revolution (PPR):** The number of encoder pulses for one complete rotation of the lead screw. This is a configurable parameter, in this case set to the default value of 2048 pulses/revolution,
- **Lead Screw Pitch:** The distance the platform covers with each complete revolution of the lead screw. This value is determined by the threading of the lead screw and, in this case, it was 2 mm.

### 2.1.3. Tensile forces measurement

The forces were measured using the WIKA F2808 miniature tensile/compressive load cells (Fig. 6c) with a rated capacity of 500 N and a relative linearity error of ±0.15% of the nominal force. These load cells were mounted on the moving platforms, secured with 3D-printed angled components on one side and connected to the clamps on the other. The load cells were linked via cables to a custom-built data acquisition system. The load cell output signals were in volts (V) rather than newtons (N). To enable the conversion of the voltage readings into force values, each load cell was individually calibrated using three reference weights with nominal masses of 2 kg, 4 kg, and 8 kg. Each reference weight was mapped to a corresponding voltage value, resulting in the determination of a polynomial equation that mapped the output signal to a force value. This calibration equation allowed accurate conversion of the voltage readings from the load cells into force measurements.

### 2.1.4. Clamping system

The setup featured four clamps (Fig. 6d), two per axis. The clamps were attached to the load cells using a metal fork connection. The fork connection permitted limited rotation of the clamps within the XY plane. This design choice was made to facilitate a uniform distribution of stresses across the textile surface.

### 2.1.5. Image capturing

The encoders discussed in Section 2.1.2 recorded the rotation of the rods driving the platform and clamp movement, and implicitly tracked the global strain between opposite clamps along each axis. However, the mechanical behaviour of the textile is more characteristic at its centre, where boundary effects are minimized. To capture strain in this region, DIC was used. This involved taking a photograph at each displacement step for subsequent analysis.

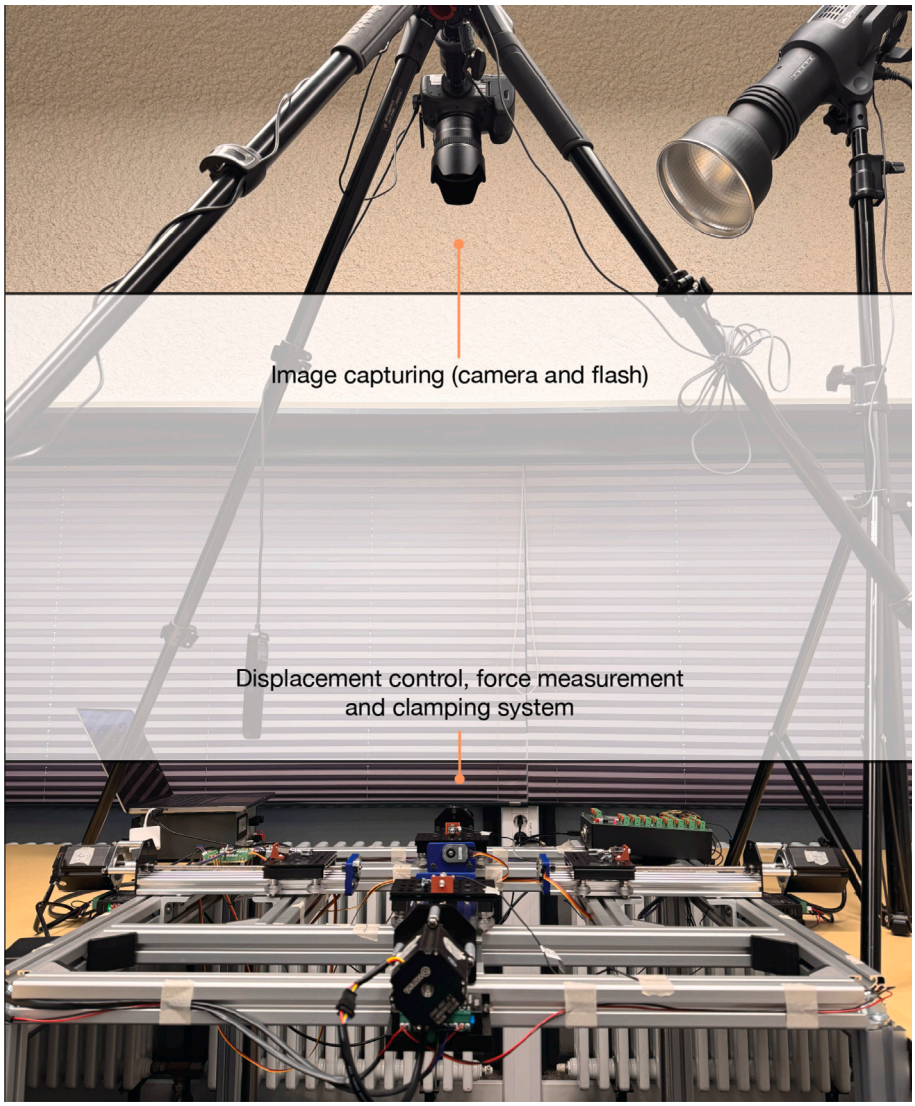


**Fig. 4.** Overview of biaxial tensile testing setup.

A Canon EOS 5DS digital camera (8688 × 5792 resolution) was positioned above the setup in such a way that the plane of the lens was parallel to the plane of the specimens. This alignment allowed the X and Y axes of the captured images to closely correspond to the course and wale directions of the textile. A 35 mm lens was used to capture a wide view of the setup, including the platforms even at maximum strain.

To minimize reflections in the photographs, which could interfere with DIC analysis (e.g., causing tracking errors), a Profoto D2 Flash was employed. The flash was positioned along the $X$-axis of the setup and directed diagonally downward onto the specimens. While the optimal position for the flash would have been directly above the test area to minimize shadows and ensure even lighting, this was not feasible due to the configuration of the setup and camera. Additionally, black matte paint was applied to the clamps to further reduce reflections.

### 2.2. Specimen preparation

The first phase of the main experimental campaign was the specimen preparation. This phase consisted of three steps: fabrication, DIC preparation and clamping. Each one of these steps was carefully executed to minimize variability between specimens.

#### 2.2.1. Specimen fabrication

Three different knitting patterns were chosen for this study. All knitting patterns were produced on a double bed and were variations of the basic interlock pattern. In this paper, they are referred to as “interlock”, “tuck”, and “hexagonal”. The interlock pattern (Fig. 7a) is a standard knitting pattern that is documented in the ISO 8388:1998 standard [26], while the other two are custom variations used previously in published architectural projects such as KnitNervi [27] and Common Thread [28]. More specifically, in the tuck pattern (Fig. 7b), the interlock pattern serves as the foundation, with every alternate knit stitch on the back needle bed being replaced by a tuck stitch. Similarly, in the hexagonal pattern (Fig. 7c), every alternate knit stitch is diagonally transferred to the back.

The specimens were fabricated on a 10.2 gauge Steiger Vega 3.130 flat-bed weft-knitting machine using recycled polyester (rPET) yarn by Morssinkhof Sustainable Products (MSP) [29]. The specimens were fabricated using a combination of black and white industrial recycled PET (rPET) yarns with a nominal linear density of 550 dtex, specifically MOPET-r Yarn 4535T (black) and MOPET-r Yarn 4835T (white), used in approximately equal proportions by weight.

The fabrication files were generated using the Steiger proprietary software. Each pattern was encoded as a bitmap image file, which was then converted into a matrix of knitting operations within the

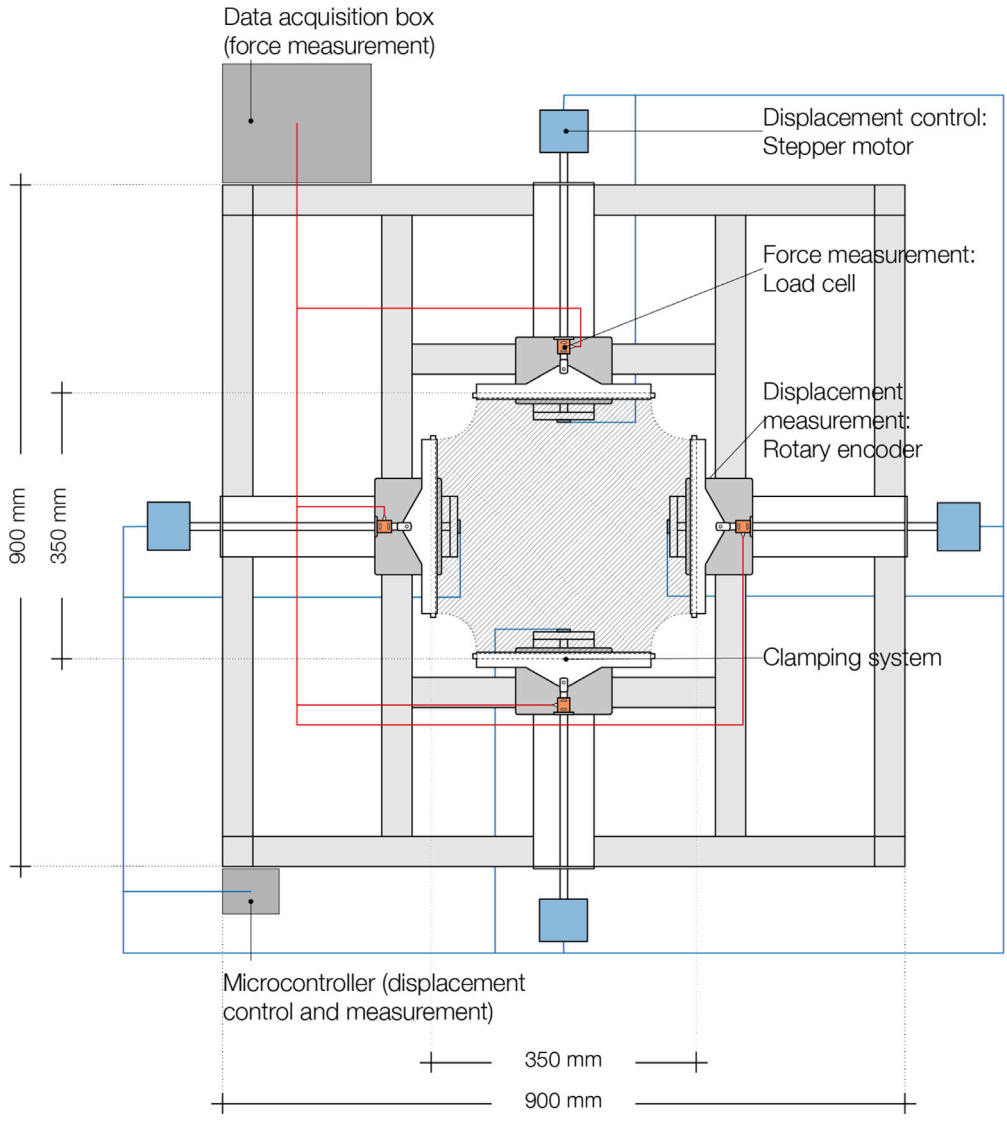


**Fig. 5.** Biaxial tensile testing setup diagram (excl. camera).

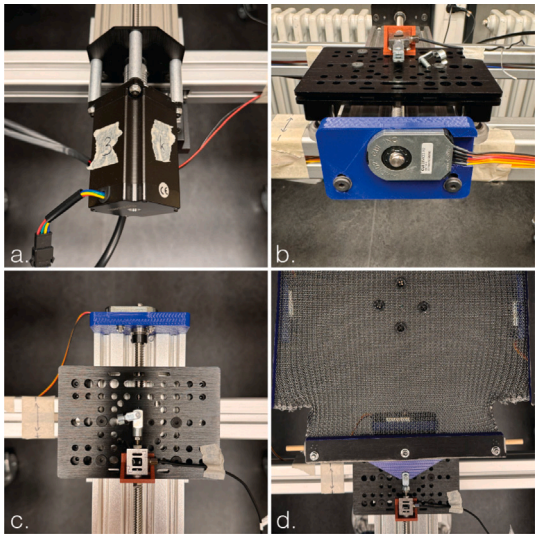


**Fig. 6.** Biaxial tensile test setup details: (a) Stepper motor; (b) Rotary encoder; (c) Moving platform, load cell and fork connection; (d) Clamping system.

machine software. The local and global properties of a CNC weft-knitted textile, including its width and height, are highly dependent on the knitting pattern; therefore, to achieve a consistent shape and size for all different patterns, a calibration process was necessary.

The specimens were designed to have a cruciform shape, which has been established in literature already since the 1950s and 1960s [30, 31]. The cruciform specimen shape satisfies the testing requirements for minimized boundary effects and a uniform biaxial stress state in the test region. A commonly used alternative, the segmented tail design, involves gripping the fabric from a series of tabs at the boundary edges [32]. However, this solution was deemed unsuitable for the current study. This was due to fabrication constraints related to weft-knitting [17], that do not apply to other materials, such as woven fabrics.

At the starting position of the biaxial setup, the area in between the clamps had an approximate size of 334 × 334 $mm^2$. Therefore, the nominal total area of the specimens, including the tails, was also set at 334 × 334 $mm^2$. The geometric composition of a specimen could be described as follows (Fig. 8a):

- **Core,** a square region at the centre of the specimen; the test area was included in the core,
- **Tails,** extensions of the core on the X and Y axes,

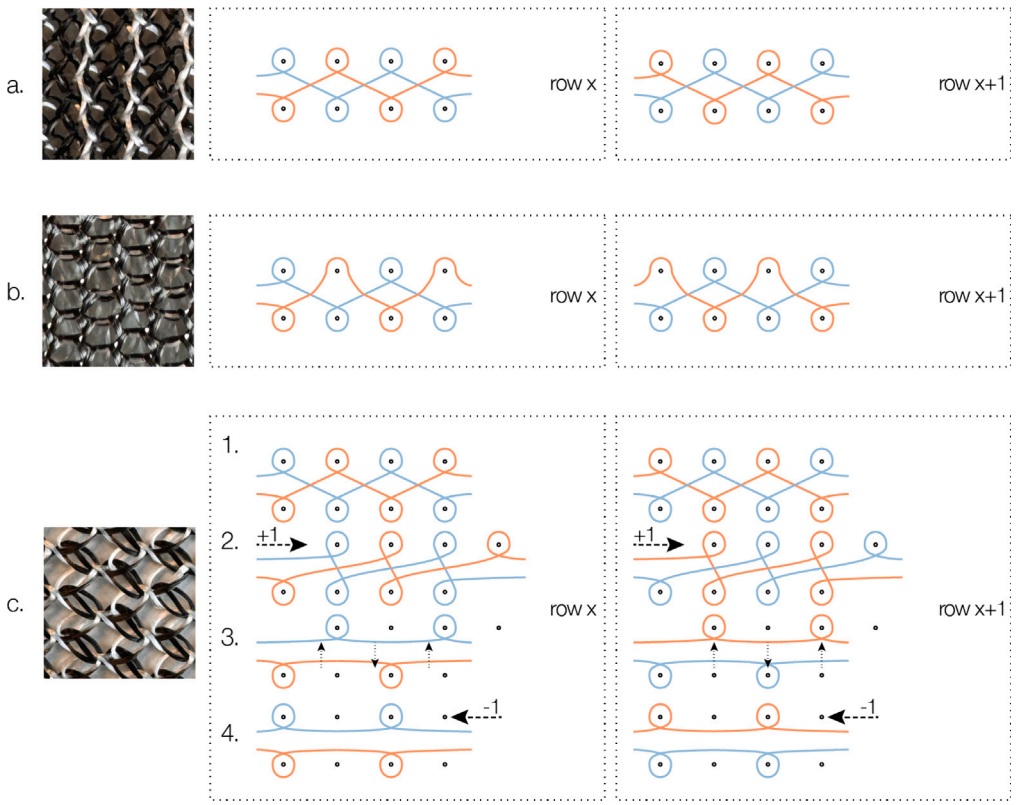


**Fig. 7.** Knitting patterns, detail photos and knitting diagrams: (a) Interlock; (b) Tuck; (c) Hexagonal.

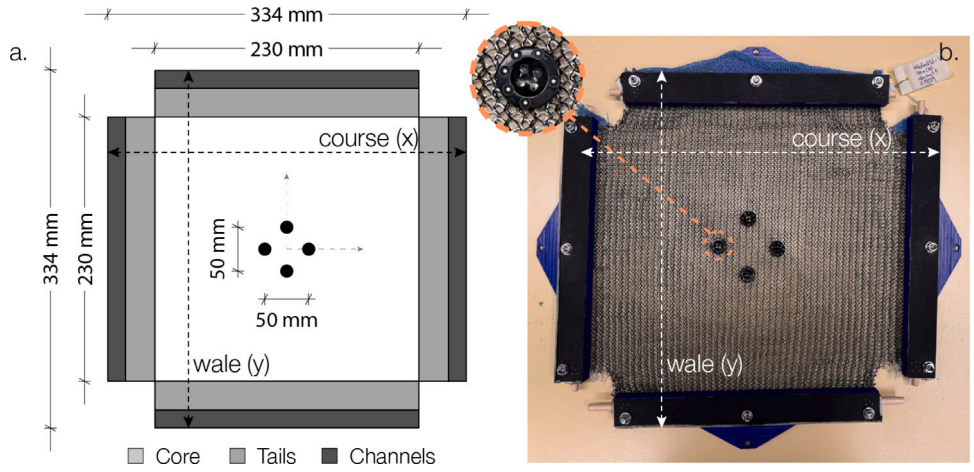


**Fig. 8.** Specimen fabrication and preparation: (a) Specimen dimensions, features and button placement; (b) DIC preparation and clamping.

- **Channels,** located at the end of the tails. These were incorporated into the textiles as functional features that facilitated the clamping process.

Furthermore, the design parameters for determining the precise shape of the cruciform specimen were as follows:

- The total width both in the course and the wale direction was set to 334 mm (Fig. 8a), corresponding to the dimensions of the area between the clamps,
- The nominal edge width both in the course and the wale direction was set to 230 mm (Fig. 8a), equal to the clamp length,
- The specimen surface needed to be taut, to avoid sagging, but not overly tensioned, to enable capturing a broader range of force–displacement pairings.

With these goals in mind, the final textile dimensions were determined through a short trial-and-error calibration process. The number of pixels per row and column representing each specimen component within the pattern bitmap is documented in Table 1.

### 2.2.2. DIC preparation

To measure strain in the core region of the specimen, four points within the test area were selected for displacement tracking with DIC. These points were positioned radially at a 2.5 cm distance (Figs. 8a,

**Table 1**
Component sizes per pattern.

| Sample name | Course size core [px] | Wale size core [px] | Course size channels [px] | Wale size channels [px] | Course size tails [px] | Wale size tails [px] |
|---|---|---|---|---|---|---|
| Interlock | 86 | 122 | 4 | 6 | 10 | 18 |
| Tuck | 76 | 152 | 4 | 6 | 6 | 22 |
| Hexagonal | 66 | 118 | 4 | 6 | 10 | 16 |

8b) from the centre of the specimen, symmetrically along both the X (course) and Y (wale) axes. Subsequently, one plastic, matte black, 14 mm diameter button (weighing approximately 0.84 g), equipped with five white stickers arranged in a polar unisymmetric pattern, was placed on each point. These stickers served as high-contrast reference points for DIC tracking. The buttons were attached to the textile using a snap-fit mechanism; this method was considered faster than alternatives such as sewing.

#### 2.2.3. Clamping

Four channels, one channel per side, were integrated into the knit architecture of each specimen. Thin timber rods of diameter 6 mm were inserted into the channels so that their midpoint aligned with an axis passing through the centre of the textile. Afterwards, the rods were placed in the clamps, aligned and fastened with three bolts to hold them tightly in place (Fig. 8b). This clamping system was considered adequate for achieving minimal slippage and textile damage, in accordance with the general requirements of ISO 13118:2024 [11].

### 2.3. Experimental procedure

At the start of each test, the moving platforms were positioned at a predefined starting location, typically at the end of the linear actuators. Following this, the load cell values were set to zero to eliminate starting noise and inconsistencies. Once the load cells were zeroed, the clamps, which had already been attached to the specimens, were secured to the setup using the fork connections. This means that the force measurements also included the in-plane forces caused by the self-weight of the clamps.

No formal preload to remove slack was applied prior to testing. However, as detailed in Section 2.2.1, the specimens were carefully designed and fabricated in such a way as to minimize sagging upon mounting. Furthermore, the force sensors were activated prior to mounting, which allowed the entire force–displacement history to be captured, including any initial forces required to engage the textile. After clamping the textiles to the setup, the camera focus was adjusted to ensure it was centred on the specimens rather than the background. This task concluded the test preparation and marked the start of the test.

Subsequently, the moving platforms advanced in predefined steps, with forces being measured using the load cells. The displacements along each half-axis, recorded by the encoders, as well as the forces along each textile edge were logged in a .csv file. At each displacement step, a photograph of the setup and specimen was taken before proceeding to the next step. For the first photograph of each test, a ruler was placed on the setup to establish the 2D scale for later analysis in the DIC software. The test continued until one of the load cells registered a force exceeding the predefined threshold of 150 N. At this point, the test was stopped, and an unloading procedure began, returning the textile to its starting position so the clamps could be safely removed. Images of the loading procedure can be found in the Appendix A (Figure A.1).

Although the load cells themselves were rated for a maximum capacity of 500 N, the 150 N threshold was conservatively set to protect the setup, particularly due to the fragility of certain mechanical components (e.g., 3D-printed angle connections) identified during preliminary testing. This precaution ensured safe and repeatable test execution across all specimens.

### 2.4. Data processing and analysis

#### 2.4.1. Force–displacement pairs

The data collected from the encoders and load cells in the setup was recorded into .csv files. From this dataset, force–displacement datapoints were generated for each specimen (defined by its knitting pattern, strain ratio, and sample number) along each half-axis. Additionally, by averaging the forces recorded in the wale and course directions, force–displacement datapoints were also created for each axis. It is important to note that the displacement recorded in this dataset corresponded to the global (clamp-to-clamp) strain. Strain analysis at the core of the specimens was conducted using DIC.

#### 2.4.2. Digital image correlation (DIC)

To perform the DIC analysis of the tensile testing for the weft-knitted textiles, the photographs captured at each displacement step were imported into ZEISS Inspect Correlate software as ‘‘deformation images’’. The 2D scale for all stages (as the steps are referred to in the software) was established using the ruler captured in the first image of each test. It is noted that in this study, DIC analysis focused exclusively on in-plane deformation in the X and Y directions. Possible displacements in the $Z$-axis due to the fabric undulation were considered negligible.

To track displacement, four physical markers (buttons) placed at the core of each specimen were used, as described in Section 2.2.2. The stickers on the buttons were designated as tracking points in the DIC software. For each button, a fitting point was computed using the Chebyshev best-fit method, which calculated the average position of the stickers and represented the effective centre of the button. The X and Y displacement of each fitting point was then tracked across all stages, relative to the reference stage (i.e., the image before the test began).

To determine the strain in the core region, the changes in distance between opposing button pairs were recorded. From these distances, the technical strain in the X and Y directions was calculated at each step relative to the reference stage (Figs. 9a-b). Additionally, the exact initial distances between the clamps along the X and Y axes were measured in the reference image, using the defined scale. These values were used for subsequent stress calculations, discussed in Section 2.4.3.

#### 2.4.3. Stress calculation

Engineering stress is commonly calculated based on the following formula:

$$\sigma = \frac{F}{A}$$

where:

- **F:** Applied force,
- **A:** Cross-sectional area of the material.

However, several challenges arise when applying this calculation to the current study. Measuring the thickness of a weft-knitted textile is particularly difficult, and the cruciform shape of the specimen, coupled with large planar strains during testing, means there is no single, well-defined cross-sectional area on which the forces act. For this study, the cross-sectional area was defined as spanning from clamp to clamp at the

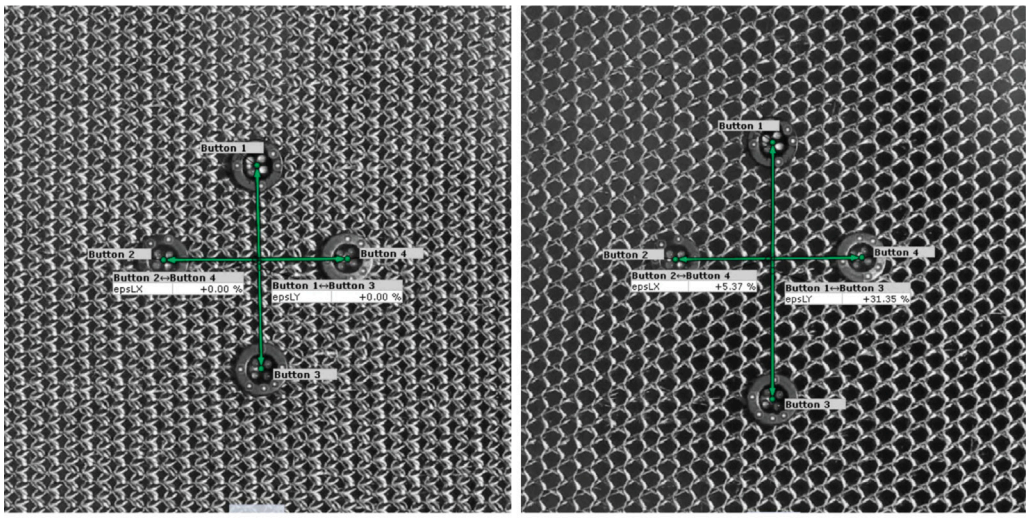


a. b.

**Fig. 9.** Digital Image Correlation (DIC) details (ratio 2:1, hexagonal pattern, sample 2): (a) Strain at reference stage; (b) Strain at final stage.

centre of the specimen, at the start of the test. This area was calculated using the following formula:

$$A = \frac{\text{Weight}}{\text{Yarn Density}} \times \frac{1}{\text{Width}}$$

where:

- **Weight:** The weight of the specimen in grams (g),
- **Yarn density:** The polyester PET yarn density in grams per cubic millimetre (g/mm$^3$), set to $1.38 \times 10^{-3}$ g/mm$^3$,
- **Width:** The size of the specimen in the examined direction (course or wale) in millimetres (mm) (Fig. 8a).

The resulting cross-sectional area was expressed in square millimetres (mm$^2$), and the engineering stress was expressed in megapascals (MPa), equivalent to newtons per square millimetre (N/mm$^2$). Specimen weights were measured using a commercial scale with an accuracy of 1 g, and the values are presented in Table 2. The course and wale widths were determined using DIC as the distances between the midpoints of the clamps along each axis at the start of the test; they are also documented in Table 2. Although these distances and the textile thickness changed during the experiment, these variations were not accounted for in the current study. This approach provides an approximation of the engineering stress, allowing for consistent analysis despite the inherent complexities of testing weft-knitted textiles under biaxial tension.

**Table 2**
Specimen weights and starting dimensions.

| Ratio | Pattern | Sample | Weight [g] | Starting course size [mm] | Starting wale size [mm] |
|---|---|---|---|---|---|
| 1:1 | Interlock | 1 | 23 | 295 | 304 |
| | | 2 | 22 | 298 | 308 |
| | | 3 | 22 | 298 | 307 |
| 1:2 | | 1 | 23 | 295 | 306 |
| | | 2 | 23 | 294 | 306 |
| | | 3 | 23 | 294 | 304 |
| 2:1 | | 1 | 23 | 295 | 307 |
| | | 2 | 23 | 295 | 307 |
| | | 3 | 23 | 297 | 305 |
| 1:1 | Tuck | 1 | 23 | 295 | 305 |
| | | 2 | 24 | 296 | 306 |
| | | 3 | 23 | 296 | 304 |
| 1:2 | | 1 | 23 | 293 | 305 |
| | | 2 | 23 | 299 | 306 |
| | | 3 | 24 | 297 | 305 |
| 2:1 | | 1 | 23 | 295 | 307 |
| | | 2 | 24 | 298 | 306 |
| | | 3 | 24 | 298 | 306 |
| 1:1 | Hexagonal | 1 | 18 | 334 | 346 |
| | | 2 | 18 | 333 | 343 |
| | | 3 | 18 | 332 | 343 |
| 1:2 | | 1 | 18 | 333 | 346 |
| | | 2 | 18 | 331 | 346 |
| | | 3 | 19 | 335 | 346 |
| 2:1 | | 1 | 18 | 336 | 347 |
| | | 2 | 18 | 334 | 346 |
| | | 3 | 18 | 334 | 346 |

## 3. Results

The results of the biaxial tensile testing of CNC weft-knitted textiles, focusing on the influence of knit architecture, strain ratio, and loading direction on the mechanical response, are presented below. The data includes force-strain and stress–strain curves, as well as a derivation and analysis of the corresponding apparent elastic moduli. Insight is provided into both the initial crimp response and the elastic behaviour of the textiles.

### 3.1. Force-strain curves

The results of the biaxial testing for three knitting patterns (interlock, tuck, and hexagonal) across three strain ratios (1:2, 1:1 and 2:1) and two loading directions (wale and course) are presented in Fig. 10. Each curve represents the average force–strain response of three samples tested under the same conditions. The majority of the resulting force-strain curves share common characteristics: an initial region of near-linear behaviour with low forces and large strains, a final near-linear region characterized by high forces and small strains, and a non-linear transitional phase connecting these two regions. The initial region can be attributed to the crimp of the specimens, where the observed strains result primarily from the geometric deformation of the textiles. This phase involves the local "unfolding" or straightening of the knitted loops, which requires relatively low tensile forces to

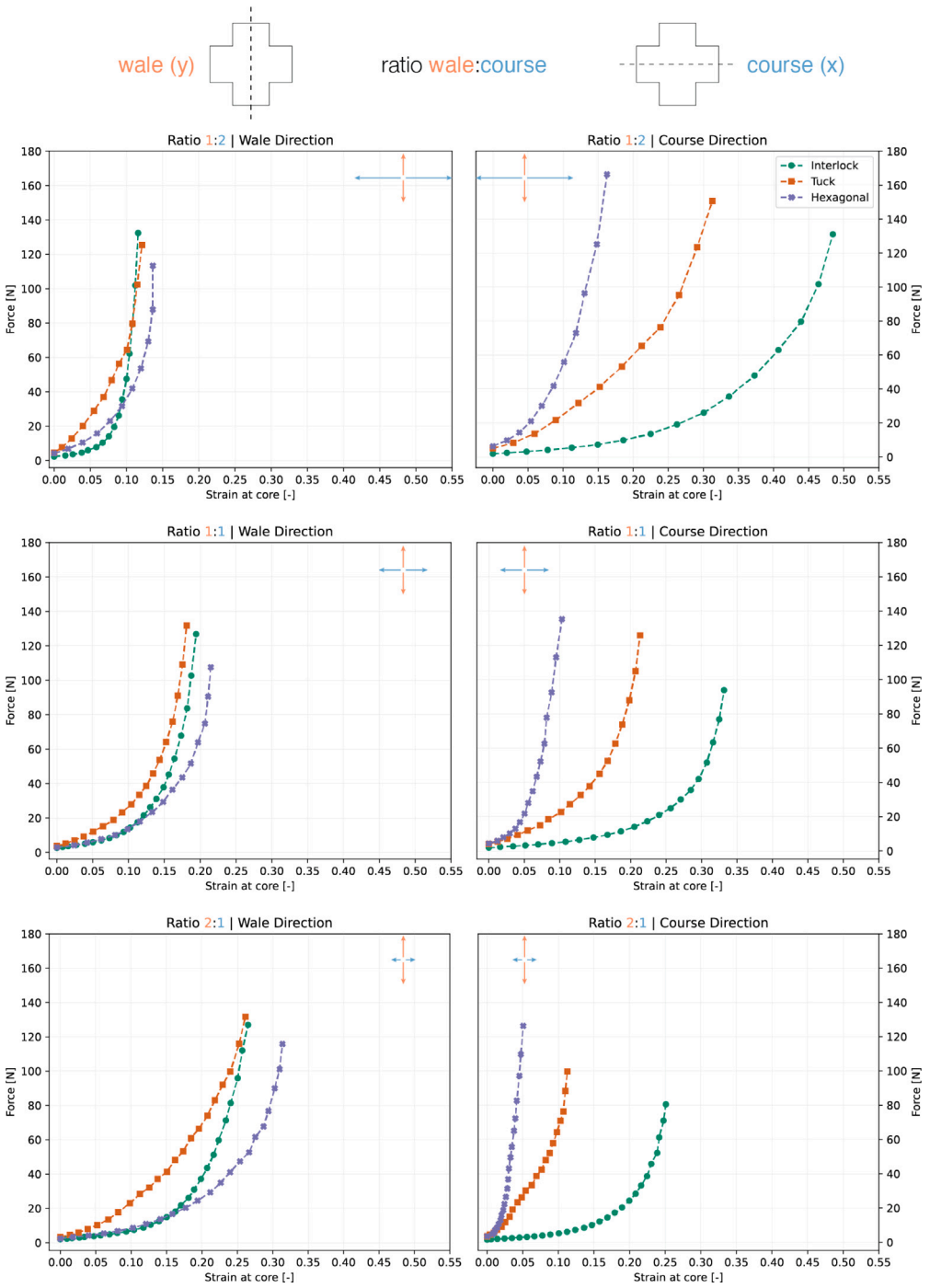


**Fig. 10.** Force–strain results per knitting direction and strain ratio.

be achieved. Furthermore, due to mechanical limitations of the setup discussed in Section 2.3, the tests did not conclude with tensile failure, and thus did not capture the complete elastic region. However, it is assumed that the phase following the crimp stage, particularly the final linear phase, represents the elastic region of the weft-knitted textiles. This phase is attributed to the elastic deformation of the yarns.

The overall tensile behaviour of the textiles varies significantly in the course direction depending on the knitting pattern. For instance, the interlock pattern exhibits a more pronounced crimp region compared to the other patterns. This suggests that the interlock allows for greater geometric deformation before reaching its fully tensioned "locked" position, after which elastic deformation begins. In contrast, the hexagonal pattern reaches the "locked" position more quickly, indicating less room for geometric deformation. In contrast, in the wale direction, although some variation is observed, the behaviour is generally more consistent across patterns.

The course and wale plots for the 1:1 strain ratio highlight the inherent anisotropy of the weft-knitted textiles: even with balanced loading conditions in two directions, the response in terms of strain differs. An important observation is that the tuck pattern seems to be the closest to an isotropic material, as its force-strain curves for the two different directions are the closest to each other. In contrast, the 1:2 and 2:1 strain ratios result in notable differences in the force-strain curves between the wale and course directions for all patterns, emphasizing the influence of directional loading.

**Table 3**
Apparent tangent and elastic moduli, reported as mean ± standard deviation (MPa).

| Ratio | Pattern | Apparent tangent modulus [MPa] | | Apparent elastic modulus [MPa] | |
|---|---|---|---|---|---|
| | | Wale | Course | Wale | Course |
| 1:2 | Interlock | 1.6 ± 0.5 | 0.6 ± 0.2 | 177.9 ± 38.5 | 31.0 ± 6.0 |
| | Tuck | 8.1 ± 1.1 | 3.9 ± 0.7 | 73.9 ± 16.9 | 22.4 ± 2.6 |
| | Hexagonal | 6.4 ± 1.7 | 8.5 ± 1.6 | 130.8 ± 25.7 | 54.9 ± 2.6 |
| 1:1 | Interlock | 1.2 ± 0.3 | 0.5 ± 0.0 | 75.1 ± 4.1 | 58.9 ± 10.8 |
| | Tuck | 3.0 ± 0.7 | 2.5 ± 0.3 | 70.0 ± 9.0 | 55.8 ± 4.5 |
| | Hexagonal | 2.4 ± 0.5 | 6.4 ± 2.0 | 138.0 ± 55.5 | 97.6 ± 31.3 |
| 2:1 | Interlock | 0.7 ± 0.0 | 0.5 ± 0.0 | 39.3 ± 8.4 | 61.8 ± 14.7 |
| | Tuck | 2.4 ± 0.5 | 4.8 ± 0.5 | 38.5 ± 9.2 | 68.7 ± 7.9 |
| | Hexagonal | 1.5 ± 0.5 | 10.0 ± 5.1 | 154.0 ± 61.4 | 157.4 ± 49.8 |

**Table 4**
Apparent tangent and elastic moduli based on global strain measurements, reported as mean ± standard deviation (MPa).

| Ratio | Pattern | Apparent tangent modulus [MPa] | | Apparent elastic modulus [MPa] | |
|---|---|---|---|---|---|
| | | Wale | Course | Wale | Course |
| 1:2 | Interlock | 1.2 ± 0.1 | 0.6 ± 0.0 | 49.0 ± 4.5 | 21.8 ± 1.9 |
| | Tuck | 7.7 ± 0.4 | 4.3 ± 0.6 | 33.2 ± 2.8 | 17.9 ± 1.0 |
| | Hexagonal | 10.7 ± 2.3 | 6.3 ± 1.3 | 50.6 ± 5.7 | 33.1 ± 3.0 |
| 1:1 | Interlock | 0.8 ± 0.0 | 0.6 ± 0.0 | 29.2 ± 0.5 | 19.6 ± 1.0 |
| | Tuck | 2.7 ± 0.6 | 2.4 ± 0.5 | 33.5 ± 2.5 | 29.2 ± 2.4 |
| | Hexagonal | 4.1 ± 0.5 | 4.6 ± 0.5 | 40.7 ± 5.8 | 50.7 ± 6.6 |
| 2:1 | Interlock | 0.4 ± 0.0 | 0.6 ± 0.1 | 25.6 ± 4.6 | 29.1 ± 5.5 |
| | Tuck | 2.1 ± 0.4 | 2.8 ± 0.5 | 28.8 ± 5.6 | 38.2 ± 5.9 |
| | Hexagonal | 2.4 ± 0.7 | 4.9 ± 0.9 | 39.3 ± 2.3 | 83.3 ± 4.8 |

### 3.2. Apparent tangent and elastic moduli

From the stress–strain curves (Fig. 11) determined using the approach described in Section 2.4.3, two moduli were derived:

- **Apparent tangent modulus:** The slope of the stress–strain curve in the crimp region, representing the apparent stiffness of the material during the geometric deformation of the textile (e.g., the unfolding of loops). In this study, the crimp region is defined by the first five data points of the stress–strain curve.
- **Apparent elastic modulus:** An estimation of the material's stiffness in the elastic region, based on the linear portion of the stress–strain curve captured during the tensile tests. In this study, the elastic modulus is derived from the last three data points of the stress–strain curve.

These moduli do not represent intrinsic material constants; instead, their values are influenced by the knit architecture, strain ratio and boundary conditions of the textiles. However, they provide valuable insights into the mechanical behaviour of the weft-knitted textiles across different deformation stages, and they are presented in Table 3 and Fig. 12.

It should be emphasized that for visualization purposes, each stress–strain curve shown in Fig. 11 represents the average response of three specimens tested under identical conditions, whereas the reported apparent moduli are calculated as the average of the individual slopes obtained from each separate stress–strain curve. As such, the values differ from the slopes of the averaged curves presented in the figure. The full stress–strain results per specimen are given in Appendix B (Figures B.1-B.9).

It is worth noting that engineering stresses are reported in this study to allow comparability with other relevant studies where engineering stresses are used. To facilitate comparison with existing literature on knitted textile properties [15,16], we provide the full force-per-unit length vs. strain data in Appendix C (Figures C.1-C.9). In this data, no assumptions are made about the cross-sectional area. Here, the unit length is defined as the nominal edge length of the specimens (Section 2.2.1).

The apparent tangent modulus ranges from 0.5 to 10.0 MPa, while the apparent elastic modulus values fall within the range of 22.4 to 177.9 MPa. For the 1:1 ratio, where both the wale and the course directions were tensioned with the same displacement step, the specimens consistently exhibit slightly greater stiffness in the wale direction. The only exception is the apparent tangent modulus of the hexagonal pattern, which is significantly higher in the course direction.

For the other two strain ratios, the direction opposite to the one tensioned at a higher rate tends to display greater stiffness. However, there are notable exceptions to this. In the hexagonal pattern, in ratio 1:2, the apparent tangent modulus is higher in the course direction, even though it was tensioned at double the rate. Similarly, in ratio 2:1, in the interlock pattern, the apparent tangent modulus is slightly lower in the course direction than in the wale direction, despite the wale being tensioned at double the rate.

Finally, the apparent elastic modulus values for the interlock and tuck patterns follow an upward trend across strain ratios from 1:2 to 2:1 in the course direction, and a downward trend in the wale direction, which aligns with expectations. This is not the case for the hexagonal pattern in the wale direction. These trends are also not consistent for the apparent tangent modulus.

### 3.3. Apparent tangent and elastic moduli based on global strain measurements

The force-strain and stress–strain curves obtained for the three knitting patterns that were presented in Sections 3.1 and 3.2 were based on strains measured at the core of the specimens using DIC. However, global (clamp-to-clamp) strains are also available, through the encoder readings at each test step. The derived apparent tangent and elastic moduli for the global strains are presented in Table 4 and Fig. 13. It is noted that these modulus values are not used to characterize material behaviour, but rather serve to illustrate the influence of boundary conditions on local deformation behaviour.

The values for the apparent tangent modulus based on global strains range from 0.6 to 10.7 MPa, which are similar to the apparent tangent modulus values as measured at the core. The apparent elastic modulus values are between 17.9 and 83.3 MPa, which is a smaller and lower range than its measured at the core counterpart. Both apparent tangent and elastic moduli are lower in the course direction in the ratio 1:2 and in the wale direction in the ratio 2:1. For the ratio 1:1, the wale direction exhibits slightly greater stiffness than the course direction in the interlock and tuck patterns, while the course direction is stiffer in the hexagonal pattern.

## 4. Discussion

The discussion interprets the findings from the biaxial tensile testing of CNC weft-knitted textiles, focusing on the role of knit architecture in determining textile stiffness. Particular attention is given to the influence of strain ratio and knitting direction, highlighting their importance in the design and assembly planning of tensile structures. Another key aspect is the interpretation of the elastic constants in relation to the strain measurement location, providing insights into how boundary conditions affect the mechanical behaviour. Finally, this section explores potential applications of the results and outlines the limitations of the study, identifying areas for future research.

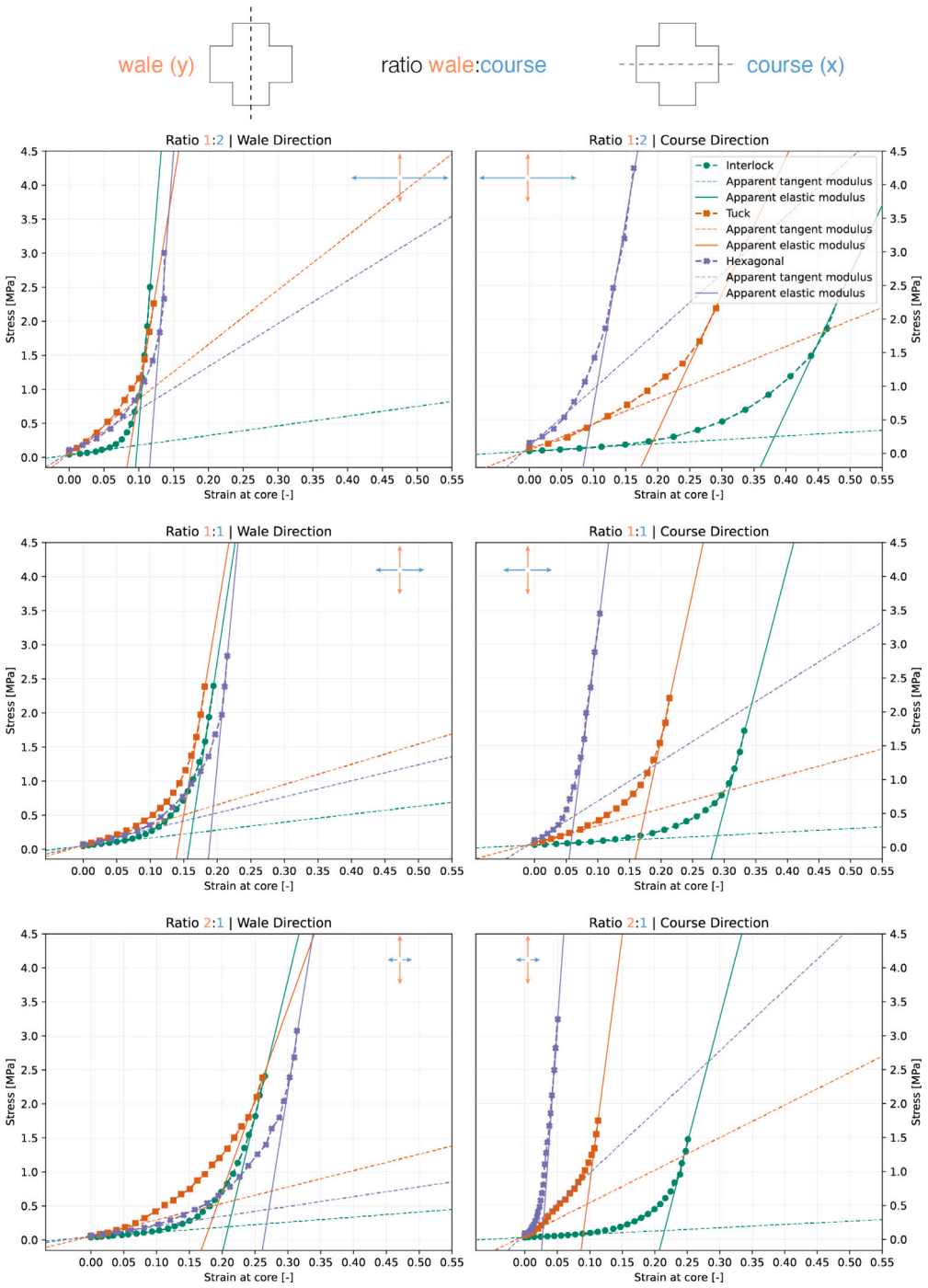


**Fig. 11.** Stress–strain results per knitting direction and strain ratio.

### 4.1. Moduli interpretation

In this study, two moduli were presented for each strain ratio, knitting pattern, and direction: the apparent tangent modulus, representing the initial crimp region, and the apparent elastic modulus, corresponding to the elastic region of the material. This distinction is crucial, as it highlights the significant behavioural differences that arise depending on the in-plane stress state (prestress) present in the textile prior to external loading, particularly in architectural and construction applications.

In the crimp region, where textiles are still highly flexible, it has been shown that small changes in applied force result in substantial strain. Therefore, for applications requiring large deformations under small applied loads, textiles should have minimal prestress. Conversely, in scenarios where deformations are undesirable, such as when textiles are used as formwork to define the shape of a final structure, prestress becomes essential. In such cases, very large forces or stresses are required to cause even minimal strain, ensuring structural integrity and shape retention.

### 4.2. Interpretation of moduli based on global strain measurements

The comparison between the apparent moduli as measured at the core versus the ones calculated using the global strain measurements reveals that for the same stresses, the strains are significantly lower at the core. Specifically, the apparent moduli at the core are typically

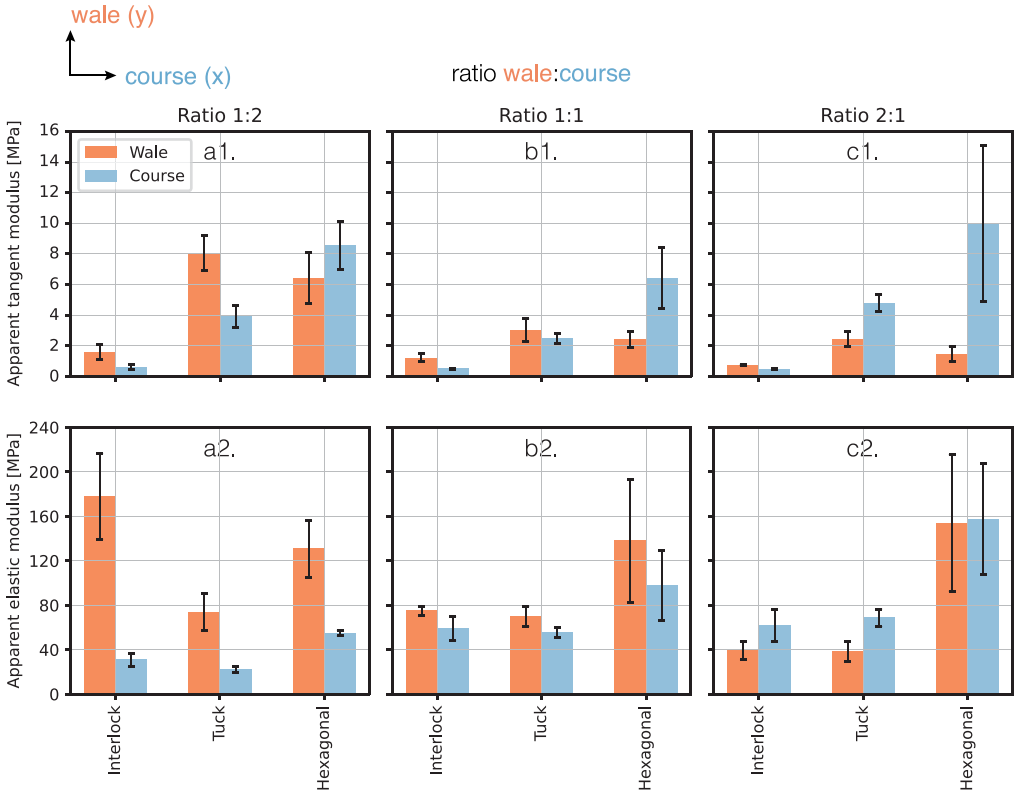


**Fig. 12.** Apparent tangent and elastic moduli per ratio, pattern and knitting direction: (a1) Apparent tangent modulus at ratio 1:2; (b1) Apparent tangent modulus at ratio 1:1; (c1) Apparent tangent modulus at ratio 2:1; (a2) Apparent elastic modulus at ratio 1:2; (b2) Apparent elastic modulus at ratio 1:1; (c2) Apparent elastic modulus at ratio 2:1.

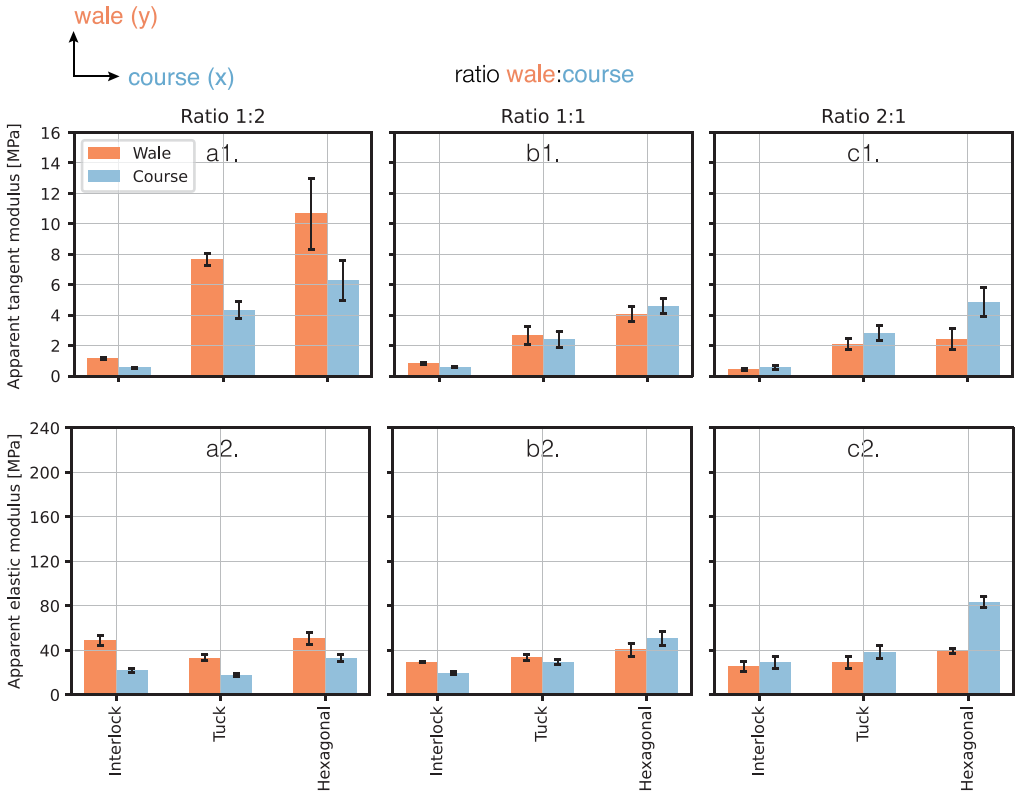


**Fig. 13.** Apparent tangent and elastic moduli per ratio, pattern and knitting direction, based on global strain measurements: (a1) Apparent tangent modulus at ratio 1:2; (b1) Apparent tangent modulus at ratio 1:1; (c1) Apparent tangent modulus at ratio 2:1; (a2) Apparent elastic modulus at ratio 1:2; (b2) Apparent elastic modulus at ratio 1:1; (c2) Apparent elastic modulus at ratio 2:1.

25%–75% higher than their global strain counterparts. This can be attributed to several factors. Firstly, the textile is physically clamped at the edges; this means that the boundaries are directly subjected to controlled displacement, leading to higher global strain values and thus lower apparent stiffness. In contrast, the core of the specimen deforms freely, as it is not restricted by local clamping. Furthermore, forces are likely to propagate in a non-uniform way through a knitted textile, due to its unique structure. Finally, although not explicitly analysed in this study, contraction in the perpendicular direction (Poisson effect) could also alter the strain distribution. Near the clamps, the displacement is primarily dictated by the applied forces, while in the core, contraction effects could reduce the apparent strain. This suggests that the stiffness of the material is not uniform across the surface but instead varies depending on its position relative to the boundaries.

### 4.3. Influence of strain ratio and knitting direction

For the 1:1 strain ratio, the specimens almost universally exhibit greater stiffness in the wale direction. This behaviour is likely due to the inherent geometrical asymmetry of knitting patterns. Examining the loop, which is the fundamental unit of knitting, reveals that there is more room for it to unfold in the course direction than in the wale direction, rendering the wale direction stiffer. An exception to this behaviour is observed in the transfer pattern, where the loops are rearranged, and the connections between them are modified through a series of transfer operations. This structural difference likely contributes to the increased stiffness in the course direction within the crimp region.

For the 1:2 and 2:1 strain ratios, the direction with the lower displacement rate tends to exhibit higher stiffness, especially in the elastic region. This is expected, as the introduction of tension in the perpendicular direction reduces flexibility in the examined direction, even in the absence of significant strain. The interlock pattern demonstrates slightly lower stiffness in the course direction for both apparent moduli, even when the wale is tensioned at double the rate. This suggests that the interlock structure is considerably more flexible in the course direction, which could potentially be counteracted by employing a strain ratio higher than 2:1.

The deviations from the expected trends per strain ratio and direction occur primarily in the crimp region, and are therefore more evident in the apparent tangent moduli. These deviations can often be attributed to the specific mesoscale structure of the knitted textiles. Depending on the knitting pattern, yarns may undergo geometric locking at different stages of the tensioning process, resulting in varying degrees of resistance in the wale and course directions. In some cases, such as the hexagonal pattern under the 1:2 strain ratio, this geometric locking appears to cause the textile to enter a linear regime earlier than expected, before the threshold of the five initial datapoints used for apparent tangent modulus calculation (as noted in Section 3.2). This can lead to an overestimation of stiffness values in the crimp region. Furthermore, while geometric deformation is taking place, differences in strain correspond to minor stress changes, making the apparent tangent modulus especially sensitive to experimental variability.

### 4.4. Comparison between different patterns

The force-strain and stress–strain results reveal the following:

- The **interlock** pattern displays higher flexibility than the other tested knitting patterns. It allows for more loop unfolding, as is evident by its prominent geometrical deformation region. Its apparent elastic modulus is relatively low, with the exception of the wale direction in the 1:1 ratio, indicating its suitability for applications requiring flexibility even at higher prestress states. It is suitable for scenarios where large deformations are acceptable or desirable, such as wearable textiles or stretchable membranes.
- The **tuck** pattern demonstrates the most isotropic behaviour under the 1:1 strain ratio, making it potentially useful in structural applications requiring balanced biaxial mechanical properties. This almost isotropy can be explained by its knit architecture, where tuck stitches are incorporated into the back layer every other needle. This renders it stiffer in the course direction and less flexible in the wale direction compared to the interlock pattern. For the 1:2 and 2:1 ratios, the wale and course directions exhibit increased stiffness, respectively, aligning with expectations.
- The **hexagonal** pattern reaches a "locked" configuration earlier in the crimp region, resulting in a consistently high apparent tangent modulus, particularly in the course direction. This indicates limited geometric deformation compared to other patterns. Its apparent elastic moduli are also higher across all strain ratios, contributing to an overall stiffer behaviour. This pattern is most suitable for applications requiring minimal deformation under loading, such as tensile structures where form retention is critical, both at low and high prestress states. Additionally, its stiffness at low strains makes it ideal for formwork applications.

### 4.5. Application

This research presents an experimental method to determine the stiffness in the crimp and elastic regions for a CNC weft-knitted textile of a specific yarn material and knit architecture. The test results can be used to determine the elastic constants of a linear-elastic phenomenological model of the textile, in which the textile is represented by an "anisotropic homogeneous continuum" [9]. They can be used as an approximation of the apparent elastic modulus required to calculate the deformation and stresses for a tensioned weft-knitted textile under specific boundary and loading conditions. This way, the structural analysis of a weft-knitted textile as part of a tensile structure could be facilitated, which is crucial for the realization of the project.

It is also noted that recording the initial geometric deformation stage and testing previously unloaded specimens are deliberate methodological choices that depart from those in earlier studies on architectural fabrics [7,33] and knitted fabrics in particular [15]. These choices offer a more detailed material understanding to support the structural design of knitted textiles; they also reflect the nature of the authors' architectural work, which often involves single-use textile deployment for formwork applications.

### 4.6. Limitations

Despite providing valuable insights into the biaxial tensile behaviour of weft-knitted textiles, this study has certain limitations that should be addressed in future work:

- **Absence of tensile failure data:** The tests were stopped before tensile failure and at a relatively low force, meaning that the full mechanical behaviour, including tensile strength and post-failure characteristics, was not captured. Therefore, the elastic region has not been fully defined, and the maximum load-bearing capacity of the textiles, which is crucial in structural applications, has not been recorded.
- **Maximum force limitation:** The maximum applied force was limited to 150 N to protect the structural integrity of the test setup. In future work, this limitation can be addressed by either upgrading the fragile mechanical components of the current setup or by transitioning to a more robust pneumatic system, enabling testing under higher force ranges.
- **Simplified stress calculations**: The calculation of engineering stress relied on assumed cross-sectional areas based on measured weight, yarn density and original size. As a result, the calculation did not account for the dynamic changes in textile thickness and cross-section during tensioning. This approximation may have introduced inaccuracies, especially at high strain levels.

- **Boundary and edge effects:** While strain was measured at the core of the specimens using DIC, the boundary stiffness might have had an effect on the overall force-strain behaviour of the specimens.
- **Limited range of knitting patterns, loading conditions and material:** The study focused on three knitting patterns, all knitted with recycled PET yarn, and a limited set of strain ratios. Expanding the range of patterns, yarn types, loading conditions and load intensity could provide a more comprehensive understanding of knitted textile behaviour.
- **DIC marker effects:** In this study, the weight of the buttons used to track strain at the specimen core (less than 1 g each) was considered negligible. Although their presence may have had a minor influence on the results, buttons were deemed to be the most reliable option for feature tracking. Alternatives such as spray painting carried a higher risk of significantly altering fabric stiffness and, consequently, the results. Future work could explore marker-free DIC methods or compare strain measurements obtained with alternative tracking approaches.

## 5. Conclusions

The study revealed significant differences in the mechanical behaviour of weft-knitted textiles under biaxial tensile testing, depending on the tested strain ratio, knitting pattern, and knitting direction. Two distinct stiffness indicators, the apparent tangent modulus and the apparent elastic modulus, were identified. These represent the stiffness of the textile in the crimp and elastic regions respectively, and the differences between them emphasize the importance of prestress in determining the response of a textile to loading in the context of a tensile structure. It was also found that the wale direction generally exhibits greater stiffness than the course direction, attributed to the inherent anisotropy of knitting patterns and the geometric characteristics of knitted loops.

Concerning the influence of the knitting pattern on the elasticity of a textile, the interlock pattern demonstrated high flexibility, particularly in the course direction, making it suitable for applications requiring large deformations or adaptability. Furthermore, the tuck pattern exhibited the most isotropic behaviour under balanced loading (1:1 strain ratio). Finally, the hexagonal pattern showed consistently high stiffness, with limited geometric deformation and high apparent elastic moduli across all strain ratios. This renders it the most suitable for applications requiring minimal deformation and high shape retention.

The strain ratio was also shown to strongly influence the mechanical response of the weft-knitted textiles. This highlights the importance of thinking critically about the assembly process while planning the building of a tensile structure. Additionally, the location of the strain measurements relative to the textile edges was also shown to influence the characterization of material stiffness. This suggests that assuming a gradient rather than a uniform stiffness across the entire surface may lead to a more accurate representation of the mechanical behaviour of the textile.

The study did not capture tensile failure, and the evolving cross-sectional area and thickness of the textiles during deformation were not considered. These limitations may impact the precision of stress calculations. Future research could explore additional knitting patterns, investigate failure mechanisms, and incorporate dynamic measurements of material properties during deformation. Advanced modelling techniques could also be used to predict the behaviour of weft-knitted textiles under complex loading conditions.

Overall, the study provided a framework for characterizing and selecting knitting patterns based on their mechanical response under specific loading conditions, facilitating the incorporation of weft-knitted textiles in architectural and construction applications. Furthermore, the experimental method presented has the potential to serve as a proof-of-concept for establishing a new benchmark; not only for the biaxial tensile testing procedure for weft-knitted textiles but also for the development of a low-cost biaxial testing setup, the preparation of test specimens and the interpretation of results. By providing a structured workflow for assessing the elastic properties of knitted textiles under biaxial loading, this approach could contribute to the development of standardized methodologies that enhance reproducibility, accuracy, and applicability in both research and industry.

## CRediT authorship contribution statement

**Nikoletta Christidi:** Writing – review & editing, Writing – original draft, Visualization, Validation, Software, Resources, Project administration, Methodology, Investigation, Formal analysis, Data curation, Conceptualization. **Christian Louter:** Writing – review & editing, Supervision. **Mariana Popescu:** Writing – review & editing, Supervision, Funding acquisition, Conceptualization.

## Declaration of AI-assisted technologies in the writing process

During the preparation of this work, the authors used ChatGPT in order to improve the readability and language of the paper. After using this tool, the authors reviewed and edited the content as needed and take full responsibility for the content of the published article.

## Declaration of competing interest

The authors declare that they have no known competing financial interests or personal relationships that could have appeared to influence the work reported in this paper.

## Acknowledgements

The authors wish to thank Giorgos Stamoulis from the TU Delft Macrolab/Stevinlaboratory, as well as Jaap Elstgeest and Sam Reus from the Department of Electronic and Mechanical Development (DEMO) at TU Delft, for their support during the design and building of the biaxial tensile testing setup.

This research was partly supported by the EIC Pathfinder programme (grant number 101162376).

## Appendix A. Supplementary data

Supplementary material related to this article can be found online at https://doi.org/10.1016/j.conbuildmat.2025.144482.

## Data availability

Data will be made available on request.

## References

[1] J. Chilton, Tensile structures - textiles for architecture and design, in: Textiles, Polymers and Composites for Buildings, Elsevier, 2010, pp. 229–257, http://dx.doi.org/10.1533/9780845699994.2.229.

[2] F. Oghazian, P. Farrokhsiar, F. Davis, A simulation process for implementation of knitted textiles in developing architectural tension structures, in: Proceedings of the IASS Annual Symposium 2021, 2021, http://dx.doi.org/10.15126/900337.

[3] M.A. Popescu, KnitCrete: Stay-in-Place Knitted Formworks for Complex Concrete Structures (Ph.D. thesis), ETH Zurich, 2019, http://dx.doi.org/10.3929/ethz-b-000408640.

[4] M. Ramsgaard Thomsen, T. Hicks, To knit a wall, knit as matrix for composite materials for architecture, in: Smart Textiles - Technology and Design, Centrum för textilforskning (CTF), The Swedish School of Textiles, University College of Borås, 2008, pp. 107–114.

[5] M.A. Popescu, M. Rippmann, A. Liew, L. Reiter, R.J. Flatt, T. Van Mele, P. Block, Structural design, digital fabrication and construction of the cable-net and knitted formwork of the KnitCandela concrete shell, Structures 31 (2021) 1287–1299, http://dx.doi.org/10.1016/j.istruc.2020.02.013.

[6] M.S. Begum, R. Milašius, Factors of weave estimation and the effect of weave structure on fabric properties: A review, Fibers 10 (74) (2022) http://dx.doi.org/10.3390/fib10090074.
[7] T. Shi, J. Hu, W. Chen, C. Gao, Biaxial tensile behavior and strength of architectural fabric membranes, Polym. Test. 82 (2020) http://dx.doi.org/10.1016/j.polymertesting.2019.106230.
[8] L. Flieger, Flexible formwork: A textile-centric approach: investigating pattern influence on the deformation behavior of weft-knitted textiles under hydrostatic loading, (MSc Thesis), Delft University of Technology, 2024.
[9] J. Uhlemann, Elastic Constants of Architectural Fabrics for Design Purposes (Ph.D. thesis), Universität Duisburg-Essen, 2016, http://dx.doi.org/10.2370/9783844044492.
[10] P. Beccarelli, Biaxial testing for fabrics and foils: optimizing devices and procedures, in: SpringerBriefs in Applied Sciences and Technology, Springer International Publishing, 2015, http://dx.doi.org/10.1007/978-3-319-02228-4.
[11] International Organization for Standardization (ISO), ISO 13118:2024, textile - biaxial tensile properties of woven fabric - determination of elasticity properties using a cruciform test piece, 2024, 13118:2024, International Organization for Standardization (ISO), [Online]. Available: https://www.iso.org/standard/84281.html.
[12] International Organization for Standardization (ISO), ISO 24281:2021, textiles - biaxial tensile properties of woven fabric - determination of maximum force and elongation at maximum force using the grab method, 2021, 24281:2021, International Organization for Standardization (ISO), [Online]. Available: https://www.iso.org/standard/78313.html.
[13] European Committee for Standardization (CEN), NEN-EN 17117-2:2021, Rubber- or plastics-coated fabrics - mechanical test methods under biaxial stress states - part 2: Determination of the pattern compensation values, 2021, 17117-2:2021, Nederlands Normalisatie-instituut (NEN), [Online]. Available: https://www.nen.nl/en/nen-en-17117-2-2021-en.
[14] European Committee for Standardization (CEN), NEN-EN 17117-1:2018, rubber or plastics-coated fabrics - Mechanical test methods under biaxial stress states - part 1: Tensile stiffness properties, 2018, 17117-1:2017, Nederlands Normalisatie-instituut (NEN), [Online]. Available: https://www.nen.nl/en/nen-en-17117-1-2019-en-247031.
[15] C. Monticelli, A. Zanelli, A. Kutlu, Design-driven uniaxial and biaxial tensile testing of knitted fabrics applied to construction, in: IABSE Symposium, Prague 2022: Challenges for Existing and Oncoming Structures, 2022, pp. 942–955, http://dx.doi.org/10.2749/prague.2022.0942.
[16] M. Tamke, A. Deleuran, C. Gengnagel, M. Schmeck, R. Cavalho, R. Fangueiro, F. Monteiro, N. Stranghöner, J. Uhlemann, M.R. Thomsen, Designing CNC knit for hybrid membrane and bending active structures, in: Textiles Composites and Inflatable Structures VII: Proceedings of the VII International Conference on Textile Composites and Inflatable Structures, CIMNE, 2015, pp. 281–295.
[17] M. Tamke, Y. Šinke, A. Deleuran, F. Monteiro, R. Fangueiro, N. Stranghöner, J. Uhlemann, M. Schmeck, C. Gengnagel, M. Thomsen, Bespoke materials for bespoke textile architecture, in: Proceedings of IASS Annual Symposia, vol. 2016, International Association for Shell and Spatial Structures (IASS), 2016, pp. 1–10.
[18] M.-S. Choi, S.P. Ashdown, Effect of changes in knit structure and density on the mechanical and hand properties of weft-knitted fabrics for outerwear, Text. Res. J. 70 (12) (2000) 1033–1045, http://dx.doi.org/10.1177/004051750007001201.
[19] R. Brad, M. Dinu, Experimental investigation on tensile strength of jacquard knitted fabrics, 2015, http://dx.doi.org/10.48550/arXiv.1510.07619.
[20] D. Semnani, Mechanical properties of weft knitted fabrics in fully stretched status along courses direction: Geometrical model aspect, Univers. J. Mech. Eng. 1 (2) (2013) 62–67, http://dx.doi.org/10.13189/ujme.2013.010205.
[21] D.B. Sitotaw, B.F. Adamu, Tensile properties of single jersey and 1× 1 rib knitted fabrics made from 100% cotton and cotton/lycra yarns, J. Eng. 2017 (2017) 1–7, http://dx.doi.org/10.1155/2017/4310782.
[22] D. Vlad, L.-I. Cioca, Research regarding the influence of raw material and knitted fabric geometry on the tensile strength and breaking elongation, Procedia Technol. 22 (2016) 60–67, http://dx.doi.org/10.1016/j.protcy.2016.01.010.
[23] S.S. Mahish, A.K. Patra, R. Thakur, Functional properties of bamboo/polyester blended knitted apparel fabrics, Indian J Fibre Text. Res. (2012).
[24] E. Eltahan, Effect of lycra percentages and loop length on the physical and mechanical properties of single jersey knitted fabrics, J. Compos. 2016 (1) (2016) http://dx.doi.org/10.1155/2016/3846936.
[25] H. Fehervary, M. Smoljkić, J. Vander Sloten, N. Famaey, Planar biaxial testing of soft biological tissue using rakes: A critical analysis of protocol and fitting process, J. Mech. Behav. Biomed. Mater. 61 (2016) 135–151, http://dx.doi.org/10.1016/j.jmbbm.2016.01.011.
[26] International Organization for Standardization (ISO), ISO 8388:1998, knitted fabrics - types - vocabulary, 1998, 8388:1998, International Organization for Standardization (ISO), [Online]. Available: https://iso.org/standard/15553.html.
[27] M. Popescu, N. Christidi, L. Scheder-Bieschin, S. Bodea, T. Van Mele, P. Block, KnitNervi: Lightness and tailored materiality for flexible concrete construction, in: Fabricate 5, 2024, http://dx.doi.org/10.3929/ETHZ-B-000707293.
[28] Common Thread, [Online]. Available: https://triennalebrugge.be/en/installations/common-thread.
[29] Industrial yarns | rPET industrial yarns | MSP Emmen, [Online]. Available: https://www.msp-emmen.com/industrial-yarns.
[30] W.D. Freeston, M.M. Platt, M.M. Schoppee, Mechanics of elastic performance of textile materials: Part XVIII. Stress-Strain Response of Fabrics Under Two-Dimensional Loading, Text. Res. J. 37 (11) (1967) 948–975, http://dx.doi.org/10.1177/004051756703701107.
[31] C. Reichardt, H. Woo, D. Montgomery, A two-dimensional load-extension tester for woven fabrics, Text. Res. J. 23 (6) (1953) 424–428, http://dx.doi.org/10.1177/004051755302300608.
[32] T.K. Ghosh, Development and evaluation of a biaxial tensile tester for fabrics, J. Test. Eval. 27 (4) (1999) 282–289, http://dx.doi.org/10.1520/JTE12225J.
[33] B. Bridgens, P. Gosling, M. Birchall, Membrane material behaviour: Concepts, practice & developments, Struct. Eng. 82 (2004) 28–33.